Impact of Aggregate–Cement Paste Reaction Forming Al-tobermorite on Ion Transport in Aged Concrete

Abudushalamu Aili[1] · Ippei Maruyama[1,2] · Yoshito Umeki[3] · Kazuhiro Yokokura[4]

Abstract

In concrete structures intended for long-term use, the diffusion properties change over time with possible chemical reactions that may happen in the concrete. In this study, we performed a two-week cesium chloride diffusion test on five cored samples from different walls in a nuclear power plant. The reaction between feldspar group aggregates and cement paste was confirmed previously. We measured the diffusion profiles of cesium and chloride ions with an electron probe microanalyzer. Cesium was adsorbed into some aggregates resulting in local minimum and maximum concentrations in the diffusion profiles. Using Fick's law, we computed the apparent diffusion coefficient, which reflects the samples' diffusion and adsorption/bound properties. The diffusion was slow in samples with lower calcium-to-alumina plus silica ratio of amorphous C-A-S-H. However, diffusion was facilitated in the samples containing the crystal form of C-A-S-H, Al-tobermorite. Such ease of diffusion could be attributed to the difference in morphology of C-A-S-H. We found that cesium adsorption is promoted with the decrease in the Ca/Si ratio and with the presence of alkali in the amorphous C-A-S-H.

Article Highlights

- Cesium chloride diffusion tests were performed on saturated samples of agedconcrete containing Al-tobermorite no Al-tobermorite
- The apparent diffusion coefficient was lower for the sample s with lower Ca/(Al+Si)in the amorphous phase of cement paste, but higher in the samples containing Al-tobermorite.
- Uptake of cesium in cement paste was higher for lower Ca/(Al+Si) ratio andpromoted with the presence of alkali.

✉ Ippei Maruyama
i.maruyama@nagoya-u.jp

1   Graduate School of Environmental Studies, Nagoya University, Nagoya, Japan

2   Graduate School of Engineering, The University of Tokyo, Tokyo, Japan

3   Civil & Architectural Engineering Department, Nuclear Power Division, Chubu Electric Power Company, Incorporated, Nagoya, Japan

4   Nuclear Safety Research & Development Center, Chubu Electric Power Company, Incorporated, Shizuoka, Japan

1 Introduction

The transport of ions in cement-based materials has been widely studied since it is one of the most common phenomena for any concrete structure whose surfaces are not perfectly coated. Invasion of ions from the surrounding environment to the concrete is susceptible to degrading the concrete's properties and reducing the structure's service life. Such degradation includes chloride-induced corrosion of reinforcing steel bars and carbonation. The invading ions first penetrate the surface of the concrete and then transport further into the internal part via the pore network by diffusion, migration, advection, and capillary suction. In saturated concrete, which is the case of the inner part of thick concrete structures, diffusion is the predominant mechanism compared with other mechanisms.

Diffusion of the ions depends on environmental factors and the material properties, especially the microstructure and chemical composition of cement paste. In Portland cement paste, the calcium silicate hydrates (C-S-H) are the main phase, accounting for more than 60% of the volume. C-S-H is composed of a central calcium oxide layer, on which silica is attached. The basic unit of attached silica is the silica dimer. The neighboring silica dimers can be connected via a silica that is called bridging silica. When the neighboring silica dimers are not connected, the general case known as empty bridging positions, interlayer calcium ions will be more concentrated in some places. As a result, the main calcium layers are winded, forming larger and smaller spaces (Gartner et al. 2017). These larger spaces are called gel pores, and the smaller spaces are called interlayer spaces. The network of gel pores, interlayer spaces, and the high specific surface area make the C-S-H the main diffusion media for invading ions. The interlayer space is regarded as a part of the solid structure, although some water/ions can be exchanged, playing a significant role in the diffusion process of ions. At the interface with water in gel pores and interlayer space, the silanol group deprotonates (i.e., loses an H^+), which is then compensated by calcium ions resulting in a positively charged surface (Lothenbach and Nonat 2015; Richardson 2014). These positively charged surfaces of C-S-H accelerate the diffusion of anions while decelerating that of cations (Goto and Roy 1981; Johannesson et al. 2007). Furthermore, the chloride ions can be physically adsorbed on C-S-H, reducing the rate of diffusion (Martín-Pérez et al. 2000). Chloride ions are also bounded chemically to other hydrates such as monosulfoaluminate (Ms) to form Friedel's salts (Georget et al. 2022; Shi et al. 2017).

Concerning the analysis and modeling of diffusion, Fick's law was applied in the beginning (Maage et al. 1996; Page et al. 1981; Thomas and Bamforth 1999). Later, improved models were developed by considering the interaction between the solid phase and ions. Specifically for chloride ions, for instance, (Martín-Pérez et al. 2000; Xi and Bazant 1999) considered the physical or chemical adsorption in the modeling. The importance of the electrical double layer that formed near the surface of C-S-H was pointed out (Elakneswaran et al. 2009; Goto and Roy 1981) and considered in (Elakneswaran et al. 2010; Friedmann et al. 2008; Samson et al. 2000). Since the interaction between various ion species that are diffusing cannot be treated independently (Gupta et al. 2019), multi-ionic diffusion models were proposed (Johannesson et al. 2007; Samson et al. 2000) and further developed (Hosokawa et al. 2011; Kari et al. 2013; Samson and Marchand 2007). Recently,

Ichikawa (2022) pointed out several shortcomings of many models, such as insufficient consideration of electrical neutrality conditions. In the same work, (Ichikawa 2022) constructed a new model for ion diffusion in porous solid with surface charge, departing only from three fundamental laws: the general theory of diffusion, Gauss's law, and electrical neutrality condition. However, complex models require sophisticated material parameters as input, compromising the applicability and accuracy of prediction. To assess the durability of concrete structures in the long term, (Sui et al. 2019) proposed a more generic approach based on multiple experimental techniques, while (Georget et al. 2023) discussed the merit of using Fick's law, which is the origin of the so-called square-root law. They suggested that Fick's law is applicable even if other phenomena, such as binding, are involved as long as equilibrium conditions are satisfied. Ichikawa 2023 also showed that the square-root law could be applied approximately for chloride diffusion in cement paste even if there are interactions between C-S-H, AFm, and diffusing chloride ions (Ichikawa et al. 2023).

Most of the studies were performed on laboratory-made cement paste and concrete samples. In engineering practice, the properties of aged concrete are different from that of laboratory-made ones after long-term use. For instance, in massive concrete walls of the decommissioning Hamaoka nuclear power plant, the cement hydrates reacted with the silica and alumina released from feldspar group aggregates after 16½ years of operation under a relative humidity higher than 80% (Rymeš et al. 2019). As a result, alumina was incorporated into C-S-H. It formed calcium aluminate silicate hydrates (C-A-S-H), whose calcium over silica (Ca/Si) molar ratio decreased (Maruyama et al. 2021). A crystal form of C-A-S-H, Al-tobermorite, was formed in the walls whose temperature was higher than ~40 °C during the operation. Such changes, i.e., changes in tortuosity of pores, reduction in the microstructural surface, and surface charge of hydrates, affect the transport of ions. Taking the alkali ions (such as sodium or potassium) which diffuse together with chloride ions, the alkali binding in C-S-H/C-A-S-H increases with the decrease in the Ca/Si molar ratio (Johannesson et al. 2007) and also with the presence of alumina (Hong and Glasser 2002). Experimental studies on such aged concrete are necessary to understand the in situ condition better and deal with accidents such as the contamination of concrete structures by radionuclides in the Fukushima accident (Tomita et al. 2021). Moreover, the obtained data also give inspiration on the diffusion of the elements after the formation of Al-tobermorite in the system of nuclear geological disposal (Dauzeres et al. 2010; Martin 1994). We performed hence cesium chloride diffusion experiment using cored concrete specimens from the walls mentioned above of the Hamaoka nuclear power plant, aiming to shed some light on the impact of the reaction forming Al-tobermorite on the diffusion properties of concrete. Since the concrete samples do not contain cesium, cesium was preferred instead of sodium or potassium. The diffusion profiles were measured by an electron probe microanalyzer (EPMA), proved to be an efficient method for evaluating the diffusion profiles (Elakneswaran et al. 2010; Mori et al. 2006).

2 Material and Method

2.1 Sample

The samples were from unit 1 of the Hamaoka Nuclear Power Plant in Omaezaki, Shizuoka Prefecture, Japan. Two samples were from internal wall #1 (IW1), and three were

from the biological shielding wall (BSW). The mixture proportions of the concrete of the two walls are given in Table 1.

Cylindrical samples with a height of 5 cm and diameter of 10 cm were cored from different locations of the walls with air-cooled dry coring to avoid any loss of ions (such as washing away calcium ions). Samples were denoted with the wall's name followed by the distance between the core center and the wall's surface: IW1-100, IW1-500, BSW-100, BSW-100, BSW-380, and BSW-1085. Maruyama et al. (2021) reported the mineral composition of these samples from quantitative XRD Rietveld analysis (see Table 2) and confirmed that aggregates dissolved and reacted with cement hydrates. Al-tobermorite was present in BSW-380 and BSW-1085, which experienced high relative humidity and mild heat during the 16.5 years of operation, but not in IW1-100, IW1-500, and BSW-100.

From the cylindrical sample of 5 cm height and 10 cm diameter, we cut a prism sample of section 15×25 mm and height of 5 cm, immersed the sample into saturated limewater, and stored at 20 °C for 28 days. We assume that the samples reached a saturated state, though there is a possibility that some pores are not yet fully saturated, as reported in the experiment (Geiker et al. 2021). After saturation, for each specimen, one surface of 15×25 mm was designated as the surface of diffusion, and all other fives surfaces were coated with epoxy (Infraguard CRJ S, Sekisui chemical co.,) which is impermeable against water.

2.2 Diffusion Experiment

After the epoxy hardening, samples were immersed in a cesium chloride solution of concentration 0.5 M. One-dimensional diffusion under such conditions continued for 15 days.

At the end of the diffusion test, we cut samples along a perpendicular direction to the diffusion surface with a diamond saw using oil as a lubricant to avoid any perturbance on the diffusion profile of cesium and chloride ions. Lubricant oil was also used during the subsequent polishing of the sample surface. The oil was washed away by ultrasonic washing in isopropanol. Then, the samples were dried and kept under a vacuum for five days before being sealed and kept for observation under an electron probe microanalyzer (EPMA).

The surface of the samples was mirror polished and coated with carbon to enhance the conductivity. Elemental distributions on the surfaces were measured using a JXA-8100 (JEOL Ltd., Japan). Measurement settings were as follows: accelerator voltage: 15 kV, probe current: 200 nA, probe diameter: 50 μm, spatial resolution (i.e., pixel size): 100×50 μm, and measurement interval: 40 ms/pixel. The elements measured in EPMA were Cs, Cl, Na, K, CaO, Si, Al, S, Fe, and Mg. Since Fe exist mainly in AFt, all of the Fe was supposed to be in the form of Fe_2O_3 and compared with Hematite as the reference. Measurement results were expressed in mass fraction of elements (Cs and Cl) or oxides (Na_2O, K_2O, CaO, SiO_2, Al_2O_3, SO_3, Fe_2O_3, and MgO).

2.3 Other Experiments for Sample Characteristics

This section presents other experiments whose results will be used to discuss the diffusion properties: porosity, relative humidity at the time of coring, reaction degree of aggregate by inductively coupled plasma atomic emission spectroscopy (ICP-AES), and Ca/(Al+Si) molar ratio of amorphous phase from energy-dispersive X-ray spectroscopy (EDS). These experiments were performed using samples of different cores from the same walls. Porosity was

Table 1 Mixture proportion of the concretes (Horiuchi et al. 1975)

Design Strength	Cement type*	Slump (cm)	Air (%)	Maximum aggregate size (mm)	Water-to-cement ratio (%)	Sand volume-to-aggregate volume ratio (%)	Cement	Water	Sand	Gravel (5–25 mm)	Water-reducing agent** (mass% per cement)
							(kg/m³-concrete)				
IW1 22.1	O	12	3.5	25	48.3	38.5	300	145	734	1178	0.750
BSW 22.1	M	12	3.5	25	48.0	39.7	300	144	758	1160	0.750

*Cement type: O: ordinary Portland cement; M: moderate-heat Portland cement (according to the Japanese Industrial Standard JIS R 5210(JSA 1973))

**Water-reducing agent: lignin-based water-reducing agent

Table 2 Phase composition of cement paste after exclusion of aggregate minerals, unit: mass% per cement paste (data from (Maruyama et al. 2021))

Sample	Amorphous phase	Portlandite	Al-tobermorite	Hydrogarnet	Ettringite	Monosulfate	Hemicarbonate	Monocarbonate	Calcite	Unhydrated clinkers
IW1-100	84.09	1.64	0.00	6.77	1.72	0.67	0.23	0.00	1.04	3.82
IW1-500	88.57	0.00	0.00	5.90	1.23	0.20	0.00	0.00	0.38	3.72
BSW-100	80.46	2.81	0.00	5.68	1.27	0.09	0.00	1.28	2.26	5.84
BSW-380	73.13	0.01	12.46	5.68	0.00	0.00	0.00	0.00	1.40	7.30
BSW-1085	84.56	0.00	4.37	4.13	0.00	0.00	0.00	0.00	0.00	6.37

measured in this study, while the others have already been presented in (Maruyama et al. 2021).

The porosity was measured using the water evaporation technique on samples of φ 100×10 mm, following the same procedure established by (Rymeš et al. 2019). The samples were first saturated in water under vacuum conditions for one hour (vacuum level 0.1 Pa) and then kept in the water bath. Their mass was periodically measured every 24 h until the difference between two subsequent measurements became less than 0.1 g. Water on the surface was wiped dry before each measurement. Apparent density was measured simultaneously using the Archimedes method. The dry state was achieved by vacuum-drying for one hour (vacuum level 0.1 Pa), followed by oven-drying at 105 °C.

Relative humidity at the time of coring was measured using samples from the air-cooling coring technique with a water activity meter (AQUALAB 4TE, METER Group) in a temperature-controlled room at 20±0.2 °C. Immediately after cutting the core to the size of φ 100×50 mm, the samples were sealed into aluminum-coated polyvinyl bags and shipped to the laboratory. In the temperature-controlled room, around 10 g of the sample was chipped from the core and sealed into aluminum–coated polyvinyl bag, roughly crushed, and then measured with the water activity meter.

The reaction degree of aggregate was determined by ICP-AES measurement on fine powder samples prepared from the mortar part of the cored samples. First, around 1 g of powder was dissolved in hydrochloric acid of 1.65 mol/L for 20 min at 20 °C. Concentrations of Ca, Si, Al, Fe, Mg, SO_4, Na, and K in the solution were measured by ICP-AES. The insoluble part was then dissolved in potassium hydroxide of 0.2 mol/L for 60 min at 60 °C. The concentration of Si in the solution was measured by ICP-AES. Summing the concentrations in hydrochloric acid and potassium hydroxide solution, we obtained the oxide composition ω^s of the soluble part of the sample. On the other hand, using the above two-step dissolution (hydrochloric acid then potassium hydroxide) method, the soluble part ω^a of fine aggregate was determined. Subtracting the soluble part of the fine aggregate from the chemical composition of the powder sample, we obtained the oxide composition of the cement paste, $\omega^p =: \omega^s - \omega^a$. These oxides ω^p in cement paste came from initial cement and reacted aggregate. Noting that the chemical composition ω^o of initial cement was known, the composition of reacted aggregate was deduced, $\omega^r =: \omega^p - \omega^o$. Appendix A.2 of (Rymeš et al. 2019) described the detailed calculation of the aggregate reaction degree.

The EDS analysis was performed on the polished surface of samples using a desktop scanning electron microscopy (AZtecOneGO EDS System, Oxford Instruments). The settings of EDS measurement were as follows: acceleration voltage of 15 kV, a working distance of 10 mm, and EDS counting 250,000 for each point. For each sample, 60 points on the amorphous phase far from the edges of mineral phases were analyzed. The results of X-ray counting were processed with ZAF matrix corrections to correct the effects of fluorescence and absorption. Atomic ratios of Ca/Si, Ca/(Al+Si), and Al/Si were computed from the average of 60 points, with standard deviation as an error bar.

The results of the above experiments are summarized in Table 3, together with the compressive strength measured on cylindrical samples according to the specifications of the Japanese Industrial Standard JIS A1149 (JSA 2017).

Table 3 Characteristics of samples: porosity, reaction degree of aggregate (from ICP-AES test), Ca/(Al + Si) molar ratio of amorphous phase (from SEM–EDS), and compressive strength (data from (Maruyama et al. 2021))

Sample	Porosity (cm^3/cm^3)	Reaction degree of aggregate (%)	Ca/Si molar ratio in amorphous phase (-)	Ca/(Al + Si) molar ratio in amorphous phase (-)	Compressive strength (MPa)
IW1-100	0.141	2.65	1.36	1.19	31.9
IW1-500	0.152	2.53	1.13	1.00	50.2
BSW-100	0.149	3.69	1.25	1.12	40.3
BSW-380	0.151	6.20	1.05	0.96	56.4
BSW-1085	0.156	5.88	0.91	0.79	74.7

3 Results of Diffusion Experiment

Combining EPMA scanning maps of CaO, SiO$_2$, and Al$_2$O$_3$ with the optical photograph of the samples, we can distinguish cement paste from aggregates. Chloride ions diffused only through cement paste, whereas cesium ions, in addition to the diffusion mainly through cement paste, were adsorbed by some aggregates in IW1-500, BSW-100, and BSW-380.

To obtain the diffusion profiles of cesium and chloride ions in the cement paste, we removed the pixels belonging to aggregates following the method presented by (Mori et al. 2006). The criteria of cement paste are expressed in the average value of 18 mm width (central part in the 25 mm of sample width) as follows: CaO < 10 mass%, 12 mass% < SiO$_2$ < 35 mass% (for IW1-100 and BSW-100) or 20 mass% < SiO$_2$ < 45 mass% (for all the other samples). The obtained distribution maps of cesium and chloride ions on cement paste are displayed in Fig. 1.

Integrating the distribution maps on cement paste along the width, we obtained the diffusion profile of cesium and chloride as a function of the diffusion distance. The diffusion profiles are shown in Fig. 2. For all the specimens, the diffusion of chloride ions was faster than that of cesium ions. Chloride molar concentration was higher than cesium all along the diffusion profile, except for the near-surface parts in the specimens BSW-380 and BSW-1085. In the sample BSW-100, a local minimum was observable around the diffusion distance of 4 mm for both cesium and chloride. We assume that this abnormality is caused by aggregate and discuss the role of aggregate in Sect. 5.3. As the article's main objective is diffusion through cement paste, we will analyze the diffusion profiles and estimate the diffusion coefficient in the next section.

4 Apparent Diffusion Coefficient

The concentration profiles in Fig. 2 are the total concentration of ions, including adsorbed/bound ions and ions in the pore solution. Hence, a binding model is required to analyze the results in Fig. 2 with advanced diffusion models accounting for the role of charged surfaces of C-A-S-H. On the other hand, Fick's law is the most straightforward way to analyze the diffusion rate. Though Fick's law oversimplifies the diffusion through C-A-S-H, it has been shown by (Georget et al. 2023) that it is still applicable when other phenomena, such as
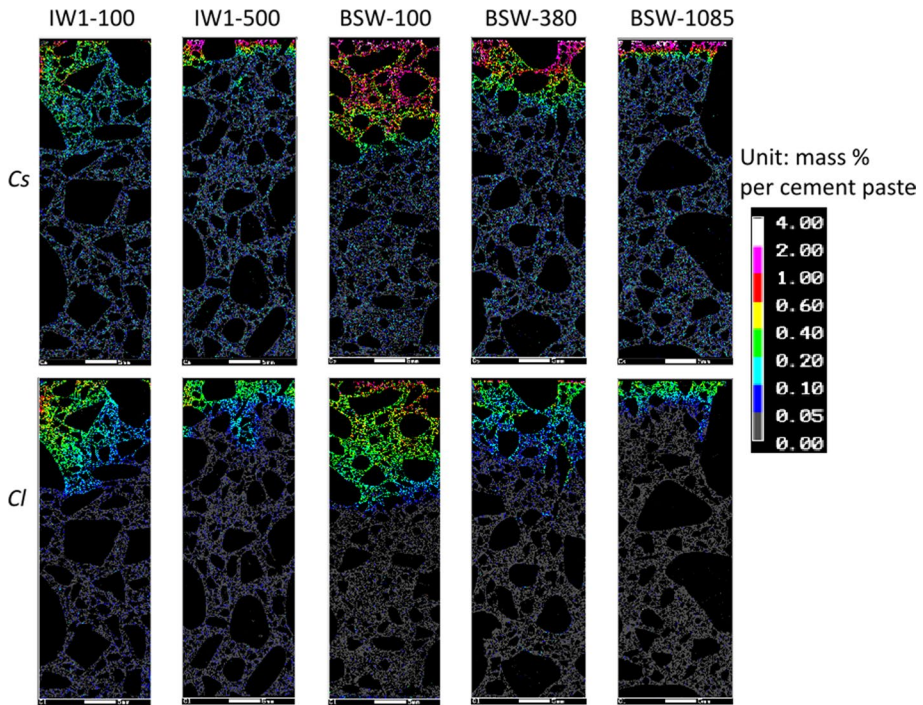
Fig. 1 Distribution maps of cesium and chloride ions in cement paste obtained from EPMA scanning by excluding aggregate

binding, are at equilibrium (i.e., not time-dependent). Thus, we analyze the results in Fig. 2 with Fick's law to obtain apparent diffusion coefficients and acknowledge that the apparent diffusion coefficient reflects an apparent behavior of the sample, including the impact of diffusion and adsorption/binding.

Fick's law states that the gradient of concentration drives diffusion. Noting the flow and concentration of ion $i(i = Cs^+, Cl^-)$ as j_i and C_i, respectively, Fick's law reads as:

$$j_i = -D_i \nabla C_i, \tag{1}$$

with D_i the diffusion coefficient of ion i. In the case of one-dimensional diffusion, like in the experiment of this study, inserting the above Fick's law of Eq. (1) into the following transport equation,

$$\frac{\partial C_i}{\partial t} = -\frac{\partial j_i}{\partial x}, \tag{2}$$

with x being the distance from the sample surface and t being the diffusion time, we obtain the standard diffusion equation:

$$\frac{\partial C_i}{\partial t} = D_i \frac{\partial^2 C_i}{\partial x^2}, \tag{3}$$
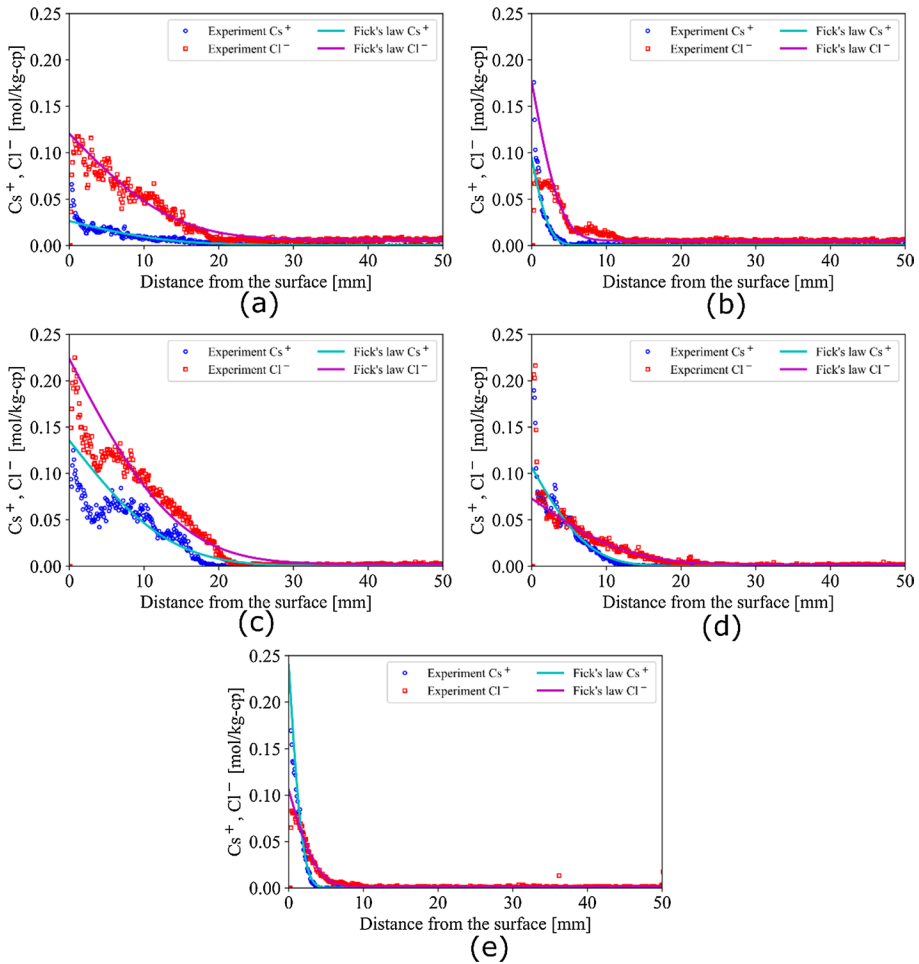
Fig. 2 Diffusion profile of cesium and chloride ions along the height of the specimens. Points are experimental results from EPMA maps, and continuous lines are fittings with Fick's law of Eq. (4)

The analytical solution of the above Eq. (3) gives us the diffusion profile of ion i at time t:

$$C_i(x,t) = C_i^0 \left(1 - erf\left(\frac{x}{2\sqrt{D_i t}} \right) \right) + C_i^\infty. \tag{4}$$

Since the concentration profile is a function of $x/\sqrt{t}$, Fick's law-based diffusion solution is also known as square-root diffusion.

In the case of the experiment, before diffusion, the initial concentrations of cesium and chloride in the samples were zero, which translates as $C_i^\infty = 0$. Fitting the measured diffusion profiles in Fig. 2 to Eq. (4), we obtained diffusion coefficients for cesium and chloride in each sample. It should be noted that, while fitting Eq. (4) to the measured ion concentration profiles, we neglected the measurement of the first 1 mm depth considering possible

calcium leaching. That is to say, the data at $x \leq 1$ mm were not included in the fitting of Eq. (4) with least square optimization method. Furthermore, we neglected the irregularities caused by aggregates, such as the local minimum near the surface in IW1-500, BSW-100, faster decrease, and the shoulder toward the diffusion front in IW1-100 and IW1-500, respectively. The results are displayed in Fig. 2, marked as Fick's law.

The above fitting gave an apparent diffusion coefficient D_i and an ionic concentration C_i^0 on the surface.

5 Discussion

5.1 Impact of Aggregate–Cement Paste Reaction on Diffusion Properties

A helpful indicator of diffusion property for engineering applications is the penetration depth. Similar to the requirement for the resistivity of concrete against chloride ion penetration (Costa and Appleton 1999; Otsuki et al. 1993), in this study, we define "the penetration depth" as the depth at which the mass concentration of ions is equal to 0.2% per mass of cement paste. Given the molar mass of chloride and cesium, 35.5 g/mol and 135 g/mol, the molar concentrations correspond to 0.056 mol/kg and 0.015 mol/kg for chloride and cesium, respectively. Considering that aggregate perturbates the experimental diffusion profiles, we computed the penetration depth from the fitted diffusion profile of Fick's law of Eq. (4).

The penetration depth of cesium and chloride ions are plotted as a function of the distance between the core center and the wall surface in Fig. 3a and compared with the penetration depth measured in a similar diffusion test on ordinary Portland cement paste with the water-to-cement ratio of 0.6 (Ichikawa et al. 2021). The penetration depths of both cesium and chloride ions are smaller for samples from the inner part of the walls. Figure 3b displays the penetration depths as a function of the relative humidity of the core at the time of coring (see Sect. 2.3). The higher the core's relative humidity at the coring time, the less deep the ions penetrate in the sample.
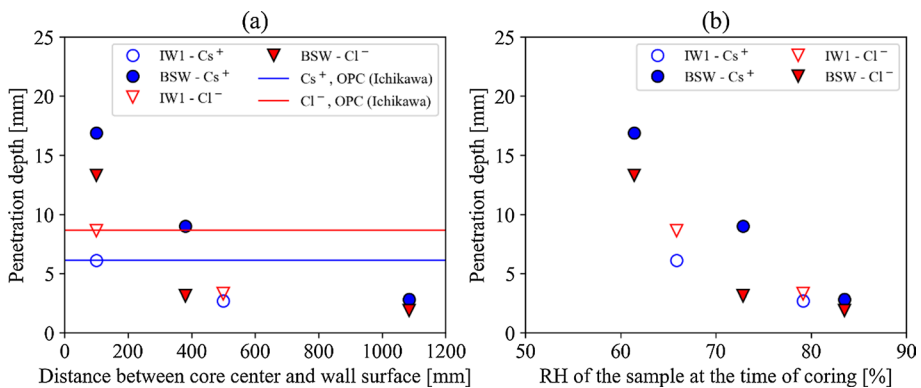

Fig. 3 Penetration depth of the ions in the function of core position **a** and relative humidity of the core at the coring **b**

Another indicator to characterize the diffusion property is the relative diffusivity λ_i, which is defined as the ratio of apparent diffusivity, measured in the experiment, over the self-diffusion coefficient D_i^{self} of the ion i in water:

$$\lambda_i = \frac{D_i}{D_i^{self}}. \tag{5}$$

The self-diffusion coefficients of chloride and cesium ions were calculated by Einstein–Stokes equation (for instance, Pau et al. 1990; Sharmilan et al. 2022)):

$$D_i^{self} = \frac{k_B T}{6\pi\eta r_i}. \tag{6}$$

where $k_B = 1.38 \times 10^{-23} \text{m}^2\text{kg} \cdot s^{-2}K^{-1}$ is Boltzmann constant, $T = 293.15K$ is temperature, $\eta = 1.0016 \times 10^{-3} \text{N} \cdot \text{m}^{-2} \cdot \text{s}$ is the dynamic viscosity of water at 20 °C, and r_i is the Stokes radius of the ion i. Taking the stokes radius of Cs^+ and Cl^- as 0.119 nm and 0.121 nm (Pau et al. 1990), the self-diffusion coefficients are found to be 1.80×10^{-9} m²/s and 1.77×10^{-9} m²/s, respectively, for Cs^+ and Cl^-.

The total porosity of these samples was very similar, differing from each other by less than 0.015 cm³/cm³ (see Table 3). Hence, we neglect the impact of porosity hereafter and assume that the difference in the diffusion properties is due to the difference in cement hydrates caused by the aggregate–cement paste reaction. Under the environmental condition, aggregates dissolved, and silica, alumina, and alkali are diffused into cement paste and react. The reaction, similar to the "post-pozzolanic reaction," refined the microstructure of the main hydrate C-A-S-H by decreasing its Ca/(Al + Si) ratio (similar to Ca/Si). The XRD results in Table 2 show that amorphous C-A-S-H accounts for around 80% of hydrates, while AFt and Ms are less than 2 and 0.7%, respectively. Thus, we suppose that the difference in diffusion properties originates from amorphous C-A-S-H.

We plot in Fig. 4 the penetration depths in the function of Ca/(Al + Si) molar ratio of amorphous C-A-S-H. Similarly, the decimal logarithm of the relative diffusivity is displayed in the function of the Ca/(Al + Si) molar ratio of the amorphous C-A-S-H in Fig. 5.

The results of samples without Al-tobermorite in Figs. 4 and 5 indicate that, with the decrease in calcium in amorphous C-A-S-H, the penetration depth decreased, as well as the relative diffusivity. The decrease in relative diffusivity with the decrease in Ca/(Al + Si) ratio has already been confirmed by experiments on cement pastes containing fly ash (Bentz et al. 2000), whereas in (Duque-Redondo et al. 2021), the contrary conclusion was drawn based on molecular dynamics. In addition to the refinement of pore structure, (Torii and Kawamura 1994) argued that the lower OH⁻ concentration in low pH cement is also a reason for the reduction in the diffusivity.

Nevertheless, such decreasing trend is disturbed when the sample contains Al-tobermorite, i.e., BSW-380 and BSW-1085. Despite a lower Ca/(Al + Si) ratio, BSW-380 shows relative diffusivity similar to BSW-100 and IW1-100. BSW-1085 shows similar relative diffusivity to that of IW1-500. It is stated in (Richardson 2004) that the morphology of C-S-H changes from fibrillar to foil-like when the Ca/Si ratio decreases. Changes in the morphology of amorphous C-S-H were observed directly in SEM images by (Maruyama 2016) on the samples submitted to long-term slow drying or heating. Also, the decrease in nitrogen specific surface area in (Maruyama et al. 2014) supported the hypothesis of morphology change. In this study, the samples containing Al-tobermorite experienced a mild temperature (~ 55 °C) for 16.5 years. Consequently,
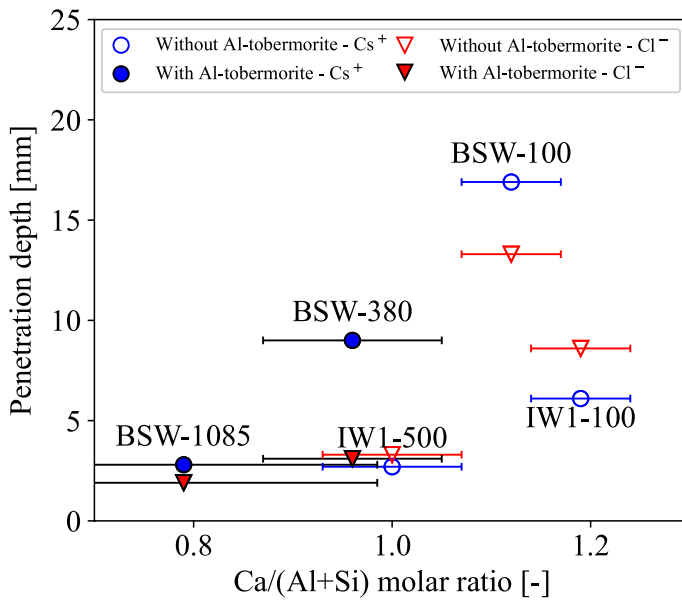
Fig. 4 Penetration depth of Cs^+ and Cl^- in the function of Ca/(Al+Si) molar ratio of the amorphous C-A-S-H

it is possible to suppose that the morphology of C-A-S-H in the samples containing Al-tobermorite differs significantly from that in the samples containing no Al-tobermorite. Figures 4 and 5 show that the critical Ca/(Al+Si) at which the morphology of C-A-S-H changes from fibrillar to foil-like might be around 1. Al-tobermorite probably formed in BSW-380 and BSW-1085 when the reaction between aggregate and cement paste progressed to a certain level that the Ca/(Al+Si) in the amorphous phase decreased below 1 and that the morphology changed from fibrillar to foil-like
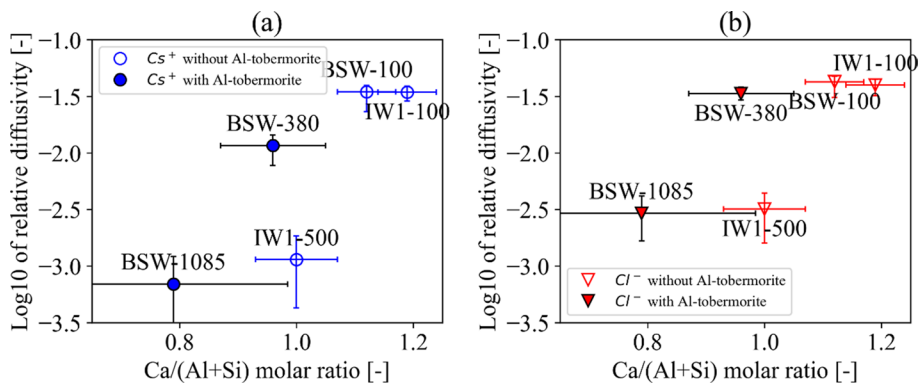
Fig. 5 Decimal logarithm of relative diffusivity Cs^+ **a** and Cl^- **b** in the function of Ca/(Al+Si) of amorphous C-A-S-H

gradually in the same time. We attribute the ease of diffusion in the samples containing Al-tobermorite to the difference in morphology of C-A-S-H. Note that Al-tobermorite, a minor phase, is not considered responsible for the increase in the relative diffusivity.

5.2 Adsorption of Cesium in Cement Paste

Since chloride ions diffuse faster than cesium ions in general, a higher molar chloride concentration than cesium is expected. However, in the measured diffusion profiles, the cesium concentration was higher near the surface in BSW-380 and BSW-1085. The shape of diffusion profiles in these two samples also confirms this higher cesium concentration. Hence, this is not caused by the irregularities near the surface. We assume that cesium ions were adsorbed on the cement paste. To compare the ability of cesium adsorption, we plotted the cesium concentration on the surface as a function of the molar ratio Ca/(Al + Si) in Fig. 6a. The results show that cesium adsorption in amorphous C-A-S-H is preferred for a lower Ca/(Al + Si) ratio.

Adsorption of cesium, more generally of alkali, by C-S-H/C-A-S-H has been studied in the literature by using synthesized C-A-S-H or by Monte Carlos simulations. (Viallis et al. 1999) studied the interaction between NaCl and CsCl solution with synthesized C-A-S-H and found that more alkali (Na$^+$, Cs$^+$) were adsorbed, while (Labbez et al. 2011) confirmed a similar trend with grand canonical Monte Carlo simulation. Experimental studies of alkali uptake by synthesized C-S-H with different Ca/Si ratios (Bach et al.2013; L'Hôpital et al. 2016) also showed similar results confirming that alkali uptake is preferred when Ca/Si is lower. For Al-tobermorite, it was found in (Shrivastava and Komarneni 1994) by experiments on synthesized tobermorite that cesium is adsorbed better in (Al + Na) substituted tobermorite than unsubstituted tobermorite, confirming the cation exchange capacity thanks to the presence of both Al and Na.

The main mechanism of cesium uptake in C-A-S-H was suggested to be an effect of charge compensation of the C-A-S-H, mainly by electrostatic interaction (Bach et al. 2013; Duque-Redondo et al. 2021). Divalent calcium ions are generally preferred over monovalent alkali ions to balance the negative charge of the C-A-S-H surface. When calcium ions in the inner space of C-S-H decrease with the decrease in Ca/Si, alkali ions would be adsorbed better (Bach et al. 2013). Thanks to their smaller solvated ionic
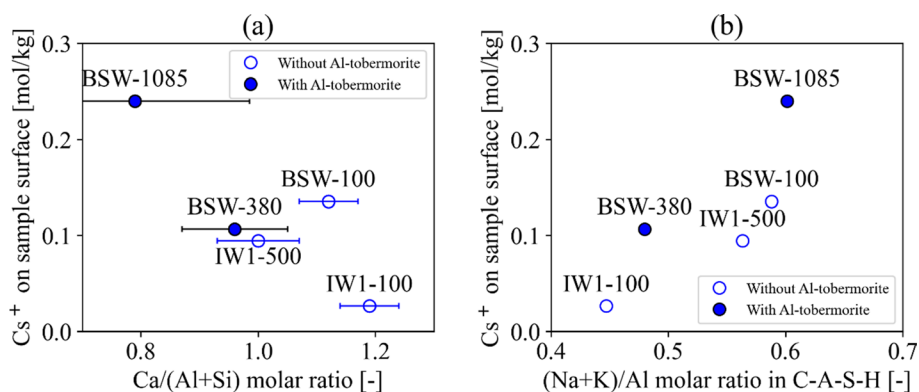

Fig. 6 Concentration of Cs^+ on the surface: **a** as a function of molar ratio Ca/(Al + Si); **b** as a function of Al/(Al + Si)

radius, cesium ions can access more interlayer surfaces of C-A-S-H compared with Na and K. In addition, with a lower enthalpy of hydration, Cs is preferred over Na and K (Bach et al. 2013). In agreement with such a mechanism, in the samples with a lower Ca/(Al + Si) ratio, the adsorption of cesium ions was promoted to such a degree that the molar concentration of cesium surpassed that of chloride.

As for the role of aluminum in the adsorption of cesium, there is a discrepancy in the literature. (Hong and Glasser 2002) suggested that the aluminum in amorphous C-A-S-H can adsorb alkali ions, while (Bach et al. 2013; L'Hôpital et al. 2016; Yan et al. 2022) did not see an increase in alkali uptake when alumina is present in synthesized C-S-H. In our experimental results, aluminum's role was also difficult to confirm when cesium concentration on the sample surface was plotted as a function of the Al/(Al + Si) ratio.

Similar to the works mentioned above on substituted tobermorite (Shrivastava and Komarneni 1994), we assume that the presence of Na and K in C-A-S-H, which were originated from the reaction between aggregate and cement paste, promoted the adsorption of cesium. We estimated the molar ratio (Na + K)/Al in C-A-S-H to check such a hypothesis. The method is as follows: Combining the inductively coupled plasma atomic emission spectroscopy measurement data and Rietveld analysis results of (Maruyama et al. 2021), we computed the alumina amount in each hydrate phase. We then took the average value of Al_2O_3 along the sample height from EPMA measurement as the total alumina and computed its portion in each hydrate. Comparing the obtained amount of alumina in C-A-S-H with Na_2O and K_2O from EPMA measurement, we estimated (Na + K)/Al molar ratio in C-A-S-H. Figure 6b displays the concentration of cesium on the sample surface in the function of the (Na + K)/Al molar ratio. Though scattered, the results show that a higher alkali content per alumina corresponds to a higher cesium concentration on the sample surface. The Na and K could be present in the interlayer space to charge balance or adsorbed on Al sites. Given two pieces of evidence: (i) Cesium can access more interlayer surface of C-A-S-H, and (ii) In the EPMA maps, distributions of Na and K along the direction of diffusion are relatively uniform, it is not possible to conclude whether the adsorption of cesium is on Al sites or in the interlayer space.

5.3 Adsorption of Cesium by Aggregates

This section discusses the adsorption of cesium by the aggregates. The original EPMA maps of cesium distribution in Fig. 1 show that cesium is adsorbed in some aggregates of samples IW1-500, BSW-100, and BSW-380. The penetration depth of cesium and the sizes of aggregates make the sample BSW-100 the best to observe cesium adsorption by the aggregates. We marked the contour of five aggregates near the surface of BSW-100 with color and numbered them on the optical photograph in Fig. 7a. The EPMA maps of cesium, Na_2O, K_2O, SiO_2, and Al_2O_3 are shown in Fig. 7b–f.

Two of the five aggregates, #4 and #5 in Fig. 7a, adsorbed cesium. In aggregate #4, cesium concentration reduced gradually from the contour of aggregate toward the center. In aggregate #5, cesium leached into from the left upper corner of the aggregate, while it can be seen that sodium leached out from the same position. Based on the EPMA maps, we estimated the chemical compositions of these aggregates and plotted them in a ternary diagram of silica, alumina, and alkali in Fig. 7g. Higher alumina content is necessary for the aggregate to adsorb cesium. However, the chemical composition is insufficient for aggregates to adsorb cesium. Aggregate #2 has a similar composition as aggregates #4 and #5, but did not adsorb cesium. The density of the aggregate, which can be roughly
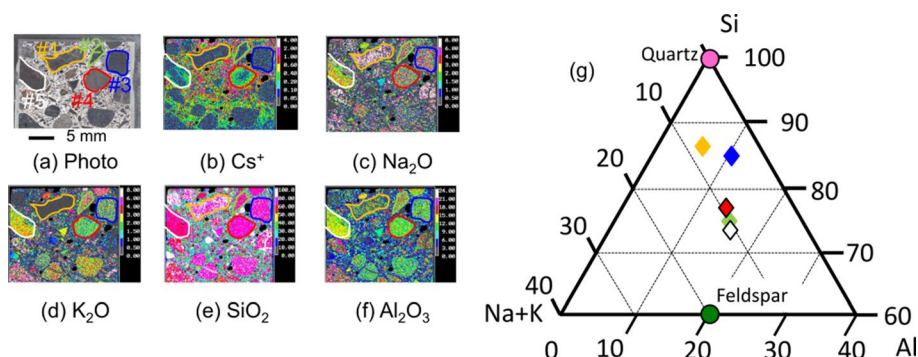
Fig. 7 Cesium adsorption on aggregate in BSW-100: (**a–f**) photograph, cesium and elemental composition of five aggregates; **g** ternary diagram (in molar ratio) showing the chemical composition of the five aggregates. Aggregate numbering–contour color: #1–orange, #2–green, #3–blue, #4–red, and #5–white. The color of diamonds in **g** corresponds to the color of the aggregate contour in (a)

distinguished from the darkness of color in the photograph (Fig. 7a), may also play a role in the cesium adsorption.

6 Conclusion

One-dimensional diffusion tests were performed for two weeks on concrete samples cored from the walls of a decommissioning nuclear power plant. Samples that experienced mild heat ~ 55 °C for 16.5 years contained Al-tobermorite while others did not. The diffusion profiles of cesium and chloride were measured using EPMA and other chemical elements in the sample. Using Fick's law, we computed an apparent diffusion coefficient that reflects the impact of diffusion and adsorption/binding. The following conclusions were drawn:

– In contrast to samples without Al-tobermorite, in which chloride concentration was higher all along the diffusion path, the cesium concentration was higher near the diffusion surface in the samples containing Al-tobermorite.
– Diffusion was slow in the samples with a lower molar ratio of $Ca/(Al+Si)$ in the amorphous C-A-S-H.
– The samples with Al-tobermorite promoted diffusion, which a difference in morphology of C-A-S-H might explain.
– Adsorption of cesium was higher in amorphous C-A-S-H with lower Ca/Si and promoted with the presence of Na and K.
– Cesium was adsorbed by aggregates that contain a higher amount of alumina. In addition to the chemical composition, the density of the aggregate may play a role in its adsorption behavior.

the National Institute for Environmental Studies, Japan, for the insightful discussions during the preparation of the manuscript.

Declarations

Conflict of interest The authors declare no conflict of interest.

References

Bach, T.T., Chabas, E., Pochard, I., Coumes, C.C., Haas, J., Frizon, F., Nonat, A.: Retention of alkali ions by hydrated low-pH cements: mechanism nd Na selectivity. Cem. Concr. Res. **51**, 14–21 (2013). https://doi.org/10.1016/j.cemconres.2013.04.010

Bentz, D.P., Jensen, O.M., Coats, A.M., Glasser, F.P.: Influence of silica fume on diffusivity in cement-based materials. I. experimental and computer modeling studies on cement pastes. Cem. Concr. Res. **30**, 953–962 (2000). https://doi.org/10.1016/S0008-8846(00)00264-7

Costa, A., Appleton, J.: Chloride penetration into concrete in marine environment-Part II: Prediction of long term chloride penetration. Mat. Struct. **32**, 354–359 (1999)

Dauzeres, A., Le Bescop, P., Sardini, P., Coumes, C.C.: Physico-chemical investigation of clayey/cement-based materials interaction in the context of geological waste disposal: Experimental approach and results. Cem. Concr. Res. **40**, 1327–1340 (2010). https://doi.org/10.1016/j.cemconres.2010.03.015

Duque-Redondo, E., Yamada, K., Manzano, H.: Cs retention and diffusion in C-S-H at different Ca/Si ratio. Cem. Concr. Res. **140**, 106294 (2021). https://doi.org/10.1016/j.cemconres.2020.106294

Elakneswaran, Y., Iwasa, A., Nawa, T., Sato, T., Kurumisawa, K.: Ion-cement hydrate interactions govern multi-ionic transport model for cementitious materials. Cem. Concr. Res. **40**, 1756–1765 (2010). https://doi.org/10.1016/j.cemconres.2010.08.019

Elakneswaran, Y., Nawa, T., Kurumisawa, K.: Influence of surface charge on ingress of chloride ion in hardened pastes. Mater. Struct. Constr. **42**, 83–93 (2009). https://doi.org/10.1617/s11527-008-9368-8

Friedmann, H., Amiri, O., Aït-Mokhtar, A.: Physical modeling of the electrical double layer effects on multispecies ions transport in cement-based materials. Cem. Concr. Res. **38**, 1394–1400 (2008). https://doi.org/10.1016/j.cemconres.2008.06.003

Gartner, E., Maruyama, I., Chen, J.: A new model for the CSH phase formed during the hydration of Portland cements. Cem. Concr. Res. **97**, 95–106 (2017).

Geiker, M., Danner, T., Michel, A., Belda Revert, A., Linderoth, O., Hornbostel, K.: 25 Years of Field Exposure of Pre-Cracked Concrete Beams; Combined Impact of Spacers and Cracks on Reinforcement Corrosion. Constr. Build. Mater. **286**, 122801 (2021). https://doi.org/10.1016/j.conbuildmat.2021.122801

Georget, F., Bénier, C., Wilson, W., Scrivener, K.L.: Chloride sorption by C-S-H quantified by SEM-EDX image analysis. Cem. Concr. Res. **152**, 1–11 (2022). https://doi.org/10.1016/j.cemconres.2021.106656

Georget, F., Wilson, W., Matschei, T.: Long-term extrapolation of chloride ingress: An illustration of the feasibility and pitfalls of the square root law. Cem. Concr. Res. **170**, 107187 (2023). https://doi.org/10.1016/j.cemconres.2023.107187

Goto, S., Roy, D.M.: Diffusion of ions through hardened cement pastes. Cem. Concr. Res. **11**, 751–757 (1981). https://doi.org/10.1016/0008-8846(81)90033-8

Gupta, A., Shim, S., Issah, L., McKenzie, C., Stone, H.A.: Diffusion of multiple electrolytes cannot be treated independently: model predictions with experimental validation. Soft Matter **15**, 9965–9973 (2019). https://doi.org/10.1039/c9sm01780a

Hong, S.Y., Glasser, F.P.: Alkali sorption by C-S-H and C-A-S-H gels: Part II. Role of Alumina. Cem. Concr. Res. **32**, 1101–1111 (2002). https://doi.org/10.1016/S0008-8846(02)00753-6

Horiuchi, M., Sugihara, K., Iwasawa, J.: Record of construction of unit 1 Hamaoka nuclear power plant. Concr. J. **13**, 11–20 (1975). https://doi.org/10.3151/coj1975.13.8_11

Hosokawa, Y., Yamada, K., Johannesson, B., Nilsson, L.O.: Development of a multi-species mass transport model for concrete with account to thermodynamic phase equilibriums. Mater. Struct. Constr. **44**, 1577–1592 (2011). https://doi.org/10.1617/s11527-011-9720-2

Ichikawa, T.: Theory of ionic diffusion in water-saturated porous solid with surface charge. J. Adv. Concr. Technol. **20**, 430–443 (2022). https://doi.org/10.3151/jact.20.430

Ichikawa, T., Haga, K., Yamada, K.: Physicochemical analysis of chloride diffusion and adsorption in water-saturated concrete : theory and measurement. J. Adv. Concr. Technol. **21**, 218–233 (2023). https://doi.org/10.3151/jact.21.218

Ichikawa, T., Yamada, K., Haga, K.: Method for predicting diffusion penetration rate of chloride ions into concrete by EPMA measurement. In: Annual Conference of Japan Cement Association. pp. 70–71 (2021)

Johannesson, B., Yamada, K., Nilsson, L.O., Hosokawa, Y.: Multi-species ionic diffusion in concrete with account to interaction between ions in the pore solution and the cement hydrates. Mater. Struct. Constr. **40**, 651–665 (2007). https://doi.org/10.1617/s11527-006-9176-y

JSA: Portland cement (JIS R5210). Tokyo, Japanese Stand. Assoc. (1973)

JSA: Method of test for static modulus of elasticity of concrete (JIS A 1149). Tokyo Japanese Stand. Assoc, (2017)

Kari, O.P., Elakneswaran, Y., Nawa, T., Puttonen, J.: A model for a long-term diffusion of multispecies in concrete based on ion-cement-hydrate interaction. J. Mater. Sci. **48**, 4243–4259 (2013). https://doi.org/10.1007/s10853-013-7239-3

L'Hôpital, E., Lothenbach, B., Scrivener, K., Kulik, D.A.: Alkali uptake in calcium alumina silicate hydrate (C-A-S-H). Cem. Concr. Res. **85**, 122–136 (2016). https://doi.org/10.1016/j.cemconres.2016.03.009

Labbez, C., Pochard, I., Jönsson, B., Nonat, A.: C-S-H/solution interface: experimental and Monte Carlo studies. Cem. Concr. Res. **41**, 161–168 (2011). https://doi.org/10.1016/j.cemconres.2010.10.002

Lothenbach, B., Nonat, A.: Calcium silicate hydrates: solid and liquid phase composition. Cem. Concr. Res. **78**, 57–70 (2015). https://doi.org/10.1016/j.cemconres.2015.03.019

Maage, M., Helland, S., Ervin, P., Vennesland, Ø., Carlsen, J.E.: Service life prediction of precast concrete structures exposed to chloride environment. Adv. Civ. Eng. **93**, 3216328 (1996). https://doi.org/10.1155/2019/3216328

Martín-Pérez, B., Zibara, H., Hooton, R.D., Thomas, M.D.A.: Study of the effect of chloride binding on service life predictions. Cem. Concr. Res. **30**, 1215–1223 (2000). https://doi.org/10.1016/S0008-8846(00)00339-2

Martin, S.I.: Synthesis of tobermorite: a cement phase expected under repository conditions. In: International High-Level Radioactive Waste Management Conference: Progress Toward Understanding. pp. 1–5., Las Vegas, NV USA, (1994)

Maruyama, I.: Multi-scale review for possible mechanisms of natural frequency change of reinforced concrete structures under an ordinary drying condition. J. Adv. Concr. Technol. **14**, 691–705 (2016). https://doi.org/10.3151/jact.14.691

Maruyama, I., Nishioka, Y., Igarashi, G., Matsui, K.: Microstructural and bulk property changes in hardened cement paste during the first drying process. Cem. Concr. Res. **58**, 20–34 (2014). https://doi.org/10.1016/j.cemconres.2014.01.007

Maruyama, I., Rymeš, J., Aili, A., Sawada, S., Kontani, O., Ueda, S., Shimamoto, R.: Long-term use of modern Portland cement concrete: the impact of Al-tobermorite formation. Mater. Des. **198**, 109297 (2021). https://doi.org/10.1016/j.matdes.2020.109297

Mori, D., Yamada, K., Hosokawa, Y., Yamamoto, M.: Applications of electron probe microanalyzer for measurement of Cl concentration profile in concrete. J. Adv. Concr. Technol. **4**, 369–383 (2006). https://doi.org/10.3151/jact.4.369

Otsuki, N., Shigeyoshi, N., Kenji, N.: Evaluation of the $AgNO_3$ solution spray method for measurement of chloride penetration into hardened cementitious matrix materials. Const. Build. Mater. **7**(4), 195–201 (1993)

Page, C.L., Short, N.R., El Tarras, A.: Diffusion of chloride ions in hardened cement pastes. Cem. Concr. Res. **11**, 395–406 (1981). https://doi.org/10.1016/0008-8846(81)90111-3

Pau, P.C.F., Berg, J.O., McMillan, W.G.: Application of stokes' law to ions in aqueous solution. J. Phys. Chem. **94**, 2671–2679 (1990). https://doi.org/10.1021/j100369a080

Richardson, I.G.: Tobermorite/jennite- and tobermorite/calcium hydroxide-based models for the structure of {C-S-H}: applicability to hardened pastes of tricalcium silicate, $β$-dicalcium silicate,

Portland cement, and blends of Portland cement with blast-furnace slag, meta. Cem. Concr. Res. **34**, 1733–1777 (2004). https://doi.org/10.1016/j.cemconres.2004.05.034

Richardson, I.G.: Model structures for C-(A)-S-H(I). Acta Crystallogr. Sect B Struct. Sci. Cryst. Eng. Mater. **70**, 903–923 (2014). https://doi.org/10.1107/S2052520614021982

Rymeš, J., Maruyama, I., Shimamoto, R., Tachibana, A., Tanaka, Y., Sawada, S., Ichikawa, Y., Kontani, O.: Long-term material properties of a thick concrete wall exposed to ordinary environmental conditions in a nuclear reactor building: the contribution of cement hydrates and feldspar interaction. J. Adv. Concr. Technol. **17**, 195–215 (2019). https://doi.org/10.3151/jact.17.195

Samson, E., Marchand, J.: Modeling the effect of temperature on ionic transport in cementitious materials. Cem. Concr. Res. **37**, 455–468 (2007). https://doi.org/10.1016/j.cemconres.2006.11.008

Samson, E., Marchand, J., Beaudoin, J.J.: Modeling the influence of chemical reactions on the mechanisms of ionic transport in porous materials. an overview. Cem. Concr. Res. **30**, 1895–1902 (2000). https://doi.org/10.1016/S0008-8846(00)00458-0

Sharmilan, S., Stang, H., Michel, A.: A multi-species reactive transport model based on ion-solid phase interaction for saturated cement-based materials. Cem. Concr. Res. **159**, 106861 (2022). https://doi.org/10.1016/j.cemconres.2022.106861

Shi, Z., Geiker, M.R., Lothenbach, B., De Weerdt, K., Garzón, S.F., Enemark-Rasmussen, K., Skibsted, J.: Friedel's salt profiles from thermogravimetric analysis and thermodynamic modelling of Portland cement-based mortars exposed to sodium chloride solution. Cem. Concr. Compos. **78**, 73–83 (2017). https://doi.org/10.1016/j.cemconcomp.2017.01.002

Shrivastava, O.P., Komarneni, S.: Cesium selectivity of (Al+Na)-substituted tobermorite. Cem. Concr. Res. **24**, 573–579 (1994). https://doi.org/10.1016/0008-8846(94)90146-5

Sui, S., Georget, F., Maraghechi, H., Sun, W., Scrivener, K.: Towards a generic approach to durability: factors affecting chloride transport in binary and ternary cementitious materials. Cem. Concr. Res. **124**, 105783 (2019). https://doi.org/10.1016/j.cemconres.2019.105783

Thomas, M.D.A., Bamforth, P.B.: Modelling chloride diffusion in concrete effect of fly ash and slag. Cem. Concr. Res. **29**, 487–495 (1999). https://doi.org/10.1016/S0008-8846(98)00192-6

Tomita, S., Haga, K., Hosokawa, Y., Yamada, K., Igarashi, G., Maruyama, I.: Modeling of the adsorption behavior of cs and sr on calcium silicate hydrates. J. Adv. Concr. Technol. **19**, 1061–1074 (2021). https://doi.org/10.3151/jact.19.1061

Torii, K., Kawamura, M.: Pore structure and chloride ion permeability of mortars containing silica fume. Cem. Concr. Compos. **16**, 279–286 (1994). https://doi.org/10.1016/0958-9465(94)90040-X

Viallis, H., Faucon, P., Petit, J.C., Nonat, A.: Interaction between salts (NaCl, CsCl) and calcium silicate hydrates (C-S-H). J. Phys. Chem. b. **103**, 5212–5219 (1999). https://doi.org/10.1021/jp983757+

Xi, Y., Bazant, Z.: Modeling chloride penetration in saturated concrete. J. Mater. Civ. Eng. **11**, 58–65 (1999)

Yan, Y., Ma, B., Miron, G.D., Kulik, D.A., Scrivener, K., Lothenbach, B.: Al uptake in calcium silicate hydrate and the effect of alkali hydroxide. Cem. Concr. Res. **162**, 106957 (2022). https://doi.org/10.1016/j.cemconres.2022.106957